



# Development of a semi-mechanistic allergenic pollen emission model

Ting Cai<sup>a,b,1</sup>, Yong Zhang<sup>a,c,1</sup>, Xiang Ren<sup>a,c</sup>, Leonard Bielory<sup>b</sup>, Zhongyuan Mi<sup>a,b</sup>, Christopher G. Nolte<sup>d</sup>, Yang Gao<sup>e</sup>, L. Ruby Leung<sup>e</sup>, Panos G. Georgopoulos<sup>a,b,c,f,g,\*</sup>

<sup>a</sup> Environmental and Occupational Health Sciences Institute (EOHSI), Rutgers University, Piscataway, NJ 08854, USA

<sup>b</sup> Department of Environmental Sciences, Rutgers University, New Brunswick, NJ 08901, USA

<sup>c</sup> Department of Chemical and Biochemical Engineering, Rutgers University, Piscataway, NJ 08854, USA

<sup>d</sup> National Exposure Research Laboratory, U.S. Environmental Protection Agency, Research Triangle Park, NC 27711, USA

<sup>e</sup> Atmospheric Sciences and Global Change Division, Pacific Northwest National Laboratory, Richland, WA 99352, USA

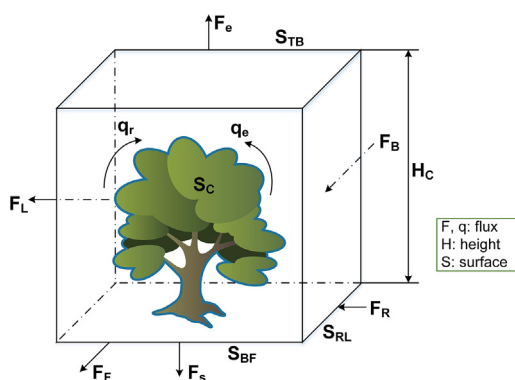
<sup>f</sup> Department of Environmental and Occupational Health, Rutgers School of Public Health, Piscataway, NJ 08854, USA

<sup>g</sup> Department of Pharmacology, Rutgers Robert Wood Johnson Medical School, Piscataway, NJ 08854, USA

## HIGHLIGHTS

- A semi-mechanistic model was developed for emission of airborne allergenic pollen.
- The model accounts for direct emission, resuspension, and meteorology influence.
- Emission pattern follows the patterns of area coverage and flowering likelihood.
- The model is robust with respect to the input parameters for oak and ragweed.

## GRAPHICAL ABSTRACT



## ARTICLE INFO

### Article history:

Received 9 July 2018

Received in revised form 15 October 2018

Accepted 17 October 2018

Available online 18 October 2018

Editor: Pavlos Kassomenos

### Keywords:

Pollen

Emission

Model

Allergy

Distribution

Sensitivity analysis

## ABSTRACT

Modeling pollen emission processes is crucial for studying the spatiotemporal distributions of airborne allergenic pollen. A semi-mechanistic emission model was developed based on mass balance of pollen grain fluxes in the surroundings of allergenic plants. The emission model considers direct emission and resuspension and accounts for influences of temperature, wind velocity, and relative humidity. Modules of this emission model have been developed and parameterized with multiple years of pollen count observations to provide pollen season onset and duration, hourly flowering likelihood, and vegetation coverage for oak and ragweed, as two examples. The simulated spatiotemporal pattern of pollen emissions generally follows the corresponding pattern of area coverage of allergenic plants and diurnal pattern of hourly flowering likelihood. It is found that oak pollen emissions start from the Southern part of the Contiguous United States (CONUS) in March and then shift gradually toward the Northern CONUS, with a maximum emission flux of  $5.8 \times 10^6$  pollen/(m<sup>2</sup> h). On the other hand, ragweed pollen emissions start from the Northern CONUS in August and then shift gradually toward the Southern CONUS. The mean ragweed emission flux during August to September can increase up to  $2.4 \times 10^6$  pollen/(m<sup>2</sup> h). This emission model is robust with respect to the input parameters for oak and ragweed. Qualitative evaluations of the model performance indicated that the simulated pollen emission is strongly correlated with the plant coverages

\* Corresponding author at: Environmental and Occupational Health Sciences Institute (EOHSI), Rutgers University, Piscataway, NJ 08854, USA.

E-mail address: [panosg@ccl.rutgers.edu](mailto:panosg@ccl.rutgers.edu) (P.G. Georgopoulos).

<sup>1</sup> Both authors contributed equally to this work.

and observed pollen counts. This model could also be applied to other pollen species given the relevant parameters.

© 2018 Published by Elsevier B.V.

## 1. Introduction

Allergenic pollen from trees, weeds and grass has been identified as one of the main triggers of Allergic Airway Disease (AAD), which affects up to 30% of the population in industrialized countries (Bielory et al., 2012; Breton et al., 2006; Cakmak et al., 2002; Sofiev and Bergmann, 2013). Air pollutants like ozone and particulate matter can act synergistically with allergenic pollen to exacerbate the AAD of allergy sufferers (Adhikari et al., 2006; Cakmak et al., 2012; Dales et al., 2004; Kim et al., 2013). Pollen emission modeling is a critical tool for investigating the release, transport and health effects of allergenic pollen.

Previous studies on pollen emission modeling are summarized in Table S1. These studies mainly focused on statistical analyses and empirical or semi-mechanistic emission models. The derived statistical relationships and empirical models of pollen emission were mainly built on the basis of observed phenology, aerobiology and meteorological and climatic factors. Kawashima and Takahashi (1999) constructed an emission model by regressing the airborne pollen data with hourly air temperature and wind speed. The emission model was then coupled with a dispersion model and wind speed extrapolated from meteorology stations to simulate the transport of cedar pollen. Schueler and Schlünzen (2006) developed an emission module by fitting the airborne pollen count and flowering time using a fourth-order polynomial curve. This emission module was then incorporated into the fifth generation Mesoscale Model (MM5) to simulate the dispersion of oak pollen.

Helbig et al. (2004) developed an empirical emission model which consists of a characteristic concentration, a lumped meteorology adjustment factor and a characteristic velocity. The characteristic concentration was parameterized using annual total emission flux and a characteristic length. The lumped meteorological adjustment factor was related to humidity, wind speed and temperature. This empirical emission model was then coupled with a mesoscale meteorology and an air quality modeling system to simulate emission and transport of hazel and alder pollen. Later, the empirical emission model was adjusted to calculate emission and transport of birch and ragweed pollen using a comprehensive model system COSMO-ART (Aerosols and Reactive Trace Substances) (Vogel et al., 2008; Zink et al., 2012). This approach was further modified by Efstathiou et al. (2011) to predict emission and transport of birch and ragweed pollen using the Community Multiscale Air Quality (CMAQ) model and the MM5 meteorology model. An emission model based on the double-threshold temperature sum was developed to simulate spatiotemporal distributions of birch pollen using the System for Integrated Modeling of Atmospheric Composition (SILAM) (Siljamo et al., 2013; Sofiev et al., 2013). A similar emission model was also applied within SILAM to simulate ragweed pollen distribution (Prank et al., 2013) and to conduct ensemble studies of birch pollen simulation using multiple meteorology and air quality models (Sofiev et al., 2015). These modeling studies provided a good starting point toward operational forecasts of pollen season onset, duration and airborne levels.

In the current study, a new semi-mechanistic emission model was developed based on mass balance of pollen grain fluxes in the surroundings of allergenic plants. This semi-mechanistic emission model incorporates information of detailed vegetation maps, the spatial distribution of start and length of pollen season, and diurnal flowering likelihood. It also accounts for influences of temperature, wind velocity and relative humidity. Different components of the emission model and their connections are illustrated in Fig. S1, and described in the methods section.

## 2. Methods

### 2.1. Emission model

The semi-mechanistic pollen emission model was constructed based on mass balance of emission fluxes surrounding the plant crowns. As shown in Fig. 1, the characteristic pollen concentrations  $C^*$  (pollen/ $m^3$ ) in the surrounding of plant crowns depend on the upward emission flux  $F_e$  (pollen/( $m^2 h$ )), resuspension flux  $q_r$  (pollen/( $m^2 h$ )), direct emission flux from plant crowns  $q_e$  (pollen/( $m^2 h$ )), deposition flux  $F_s$  (pollen/( $m^2 h$ )), and lateral emission fluxes  $F_L$ ,  $F_R$ ,  $F_B$  and  $F_F$  (pollen/( $m^2 h$ )). This mass balance of pollen grains is governed by Eq. (1),

$$H_C S_{TB} \frac{dC^*}{dt} = (F_R - F_L) S_{RL} + (F_B - F_F) S_{BF} - F_e S_{TB} - F_s (S_{TB} + S_C) + K_e q_e S_C + K_r q_r (S_{TB} + S_C) \quad (1)$$

where  $H_C$  (m) is the plant height.  $S_{TB}$ ,  $S_{RL}$  and  $S_{BF}$  ( $m^2$ ) are the areas of the top, left and back surface of the model box, respectively.  $S_C$  ( $m^2$ ) is the surface area of the plant crowns.  $K_e$  and  $K_r$  (dimensionless) are the lumped meteorology adjustment factors for direct emission and resuspension fluxes, respectively. The 4th and 6th terms on the right side of Eq. (1) reflect the assumption that resuspension flux comes from pollen deposited on a crown of a plant and the nearby ground covered by this plant.

During the pollen season, two assumptions can be made: (1) quasi-steady state for mass transfer of pollen grains in the immediate surrounding of the plant crowns (i.e.,  $\frac{dC^*}{dt} = 0$ ); and (2) a quasi-equilibrium balance of the lateral emission fluxes (i.e.,  $F_L = F_R$ ,  $F_B = F_F$ ). On the basis of these two assumptions, Eq. (1) can be reduced to:

$$F_e + F_s (1 + LAI) = K_e q_e LAI + K_r q_r (1 + LAI) \quad (2)$$

where  $LAI$  (dimensionless) is the Leaf Area Index which, according to the definition, can be used to approximate the quantity  $\frac{S_C}{S_{TB}}$ .

The upward emission flux  $F_e$  and the deposition emission flux  $F_s$  can also be calculated using the deposition velocity  $v_d$  and a

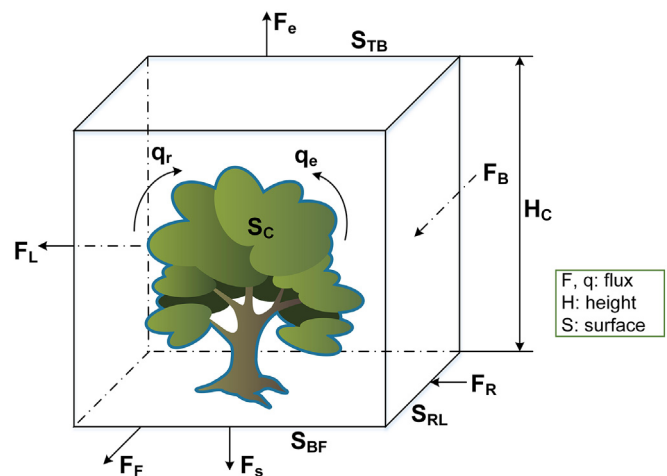


Fig. 1. Schematic diagram of emission model of pollen grains.

characteristic velocity  $u_*$  in the near surrounding of plant crowns according to Eq. (3):

$$\begin{cases} F_e = C^* u_* \\ F_s = C^* v_d \end{cases} \quad (3)$$

In the current study,  $u_*$  is approximated using the friction velocity from Weather Research and Forecasting (WRF) model output files. This follows the approach reported in the literature (Efstathiou et al., 2011; Helbig et al., 2004).

The resuspension emission  $q_r$  can be associated with the direct emission flux  $q_e$  through a proportionality factor  $C_r$  (dimensionless) as shown in Eq. (4):

$$\begin{cases} q_e = q_p L_d L_h \\ q_r = C_r q_e \end{cases} \quad (4)$$

where  $q_p$  (pollen/(m<sup>2</sup> year)) is the total number of pollen grains emitted per unit area during a pollen season, which can generally be measured or obtained from aerobiology literature.  $L_d$  (%) and  $L_h$  (%) are the daily and hourly flowering likelihood, respectively.

The upward emission flux  $F_e$  can thus be solved through the combination of Eqs. (1) to (4). The resultant upward emission flux  $F_e$  is given by:

$$F_e = \frac{q_p L_d L_h (K_e LAI + C_r K_r (1 + LAI))}{1 + v_d (1 + LAI)/u_*} \quad (5)$$

**Table 1**

Parameters for pollen emission model. These parameters were derived from the literature, and also used for global sensitivity analysis.

Parameter and ID	Oak	Ragweed
1 $H_c$ , plant height (m)	30 <sup>a</sup>	0.69 <sup>b</sup>
2 $C_r$ , proportional factor (unitless)	0.7 <sup>c</sup>	0.7 <sup>c</sup>
3 $q_p$ , annual emission flux (pollen grain/(m <sup>2</sup> year))	1.0 × 10 <sup>9d</sup>	2.8 × 10 <sup>9e,f</sup>
4 $LAI$ , Leaf Area Index (m <sup>2</sup> /m <sup>2</sup> )	3.4 <sup>h</sup>	1.2 <sup>i</sup>
5 $u_*$ , friction velocity (m/s)	WRF data <sup>j</sup>	WRF data <sup>j</sup>
6 $c_{Te}$ , $c_{Ue}$ , $c_{Ve}$ , correction factor for direct emission (unitless)	1 <sup>c</sup>	1 <sup>c</sup>
7 $c_{Ur}$ , $c_{Vr}$ , correction factor for resuspension (unitless)	1 <sup>c</sup>	1 <sup>c</sup>
8 $T_{te}$ , threshold temperature for direct emission (°C)	10 <sup>c</sup>	0 <sup>k</sup>
9 $U_{te}$ , threshold relative humidity for direct emission (%)	60 <sup>c</sup>	60 <sup>c</sup>
10 $V_{te}$ , threshold velocity for direct emission (m/s)	2.65 <sup>c</sup>	2.9 <sup>k</sup>
11 $U_{tr}$ , threshold relative humidity for resuspension (%)	85 <sup>c</sup>	85 <sup>c</sup>
12 $V_{tr}$ , threshold velocity for resuspension (m/s)	0.9 <sup>c</sup>	0.9 <sup>c</sup>
13 $r_a$ , aerodynamic resistance (h/m)	Eq. (17)	Eq. (17)
14 $r_b$ , quasi-laminar resistance (h/m)	Eq. (17)	Eq. (17)
15 $v_s$ , settling velocity (m/s)	Eq. (15)	Eq. (15)
16 $P_c$ , percentage of area coverage (%)	BELD 3.1	Eq. (7)
17 $L_d$ , daily flowering likelihood (%)	Eq. (8)	Eq. (8)
18 $L_h$ , hourly flowering likelihood (%)	Eq. (9)	Literature <sup>l</sup>
19 $u_{*t}$ , threshold friction velocity (m/s)	Eq. (10)	Eq. (10)
20 $z_0$ , surface roughness (m)	10 <sup>m</sup>	0.1 <sup>m</sup>
21 $d_p$ , diameter of pollen grain (μm)	28 <sup>n</sup>	18 <sup>n</sup>
22 $\rho_p$ , density of pollen grain (kg/m <sup>3</sup> )	1200 <sup>n</sup>	1280 <sup>n</sup>
23 $C_s$ , slip correction factor (unitless)	1.008 <sup>m</sup>	1.008 <sup>m</sup>

<sup>a</sup> Brose et al. (1999).

<sup>b</sup> Chamecki et al. (2009).

<sup>c</sup> Helbig et al. (2004).

<sup>d</sup> Schueler and Schlünzen (2006).

<sup>e</sup> Foster et al. (1980).

<sup>f</sup> Fumanal et al. (2007).

<sup>h</sup> Wang et al. (1992).

<sup>i</sup> Deen et al. (2001).

<sup>j</sup> Nolte et al. (2018) and Spero et al. (2016).

<sup>k</sup> Zink et al. (2012).

<sup>l</sup> Martin et al. (2010).

<sup>m</sup> Seinfeld and Pandis (1997).

<sup>n</sup> Davis and Brubaker (1973).

where all the terms on the right side can either be measured, or parameterized and approximated through measurable factors.

The pollen emission flux in a cell of the modeling grid can thus be calculated through:

$$F_g = F_e P_c \quad (6)$$

where  $P_c$  (%) is the percentage of area coverage of allergenic plants in the corresponding cell of the modeling grid. Each of the terms in Eqs. (5) and (6) are listed in Table 1 and described in the following subsections.

## 2.2. Vegetation coverage

The area coverage of oak was derived from the Biogenic Emissions Land Use Database, version 3.1 (BELD3.1) (Kinnee et al., 1997). The area coverage for oak across the Contiguous United States (CONUS) was generated using Spatial Allocator to redistribute the BELD3.1 data with 1-km grid resolution into 36-km grid resolution (Eyth and Habisak, 2003).

The area coverage of ragweed was generated using an algorithm developed on the basis of observed ragweed pollen counts and vegetation coverage information from BELD3.1. This is a two-stage algorithm similar to the methods reported in the literature (Fig. S2) (Csornai et al., 2010; Pauling et al., 2012; Skjøth et al., 2010). The first stage is to estimate the ragweed plant coverage in the grid cells that contain a monitoring station collecting the ragweed pollen count, and to identify the relationship between ragweed coverage and relevant land use and land coverage. The second stage is to estimate the ragweed plant coverage in the remaining grid cells using the relationship established in the first stage. Observed daily ragweed pollen counts were obtained from all available monitoring stations of the National Allergy Bureau (NAB) of the American Academy of Allergy, Asthma and Immunology (AAAAI) during the period of 1994–2010 across the CONUS (Fig. S3). Two neighboring Canadian monitoring stations were also included in the current study to augment these data. The main climate characteristics and geographical locations of the studied stations are listed in Table S2. It was found that the mean annual production of ragweed pollen was mainly relevant to area coverages of grass land, crop grass land, and savanna land.

The estimation of ragweed plant coverage in a cell of the modeling grid was generated using:

$$P_R = b_G P_G + b_{CG} P_{CG} + b_{Sa} P_{Sa} \quad (7)$$

where  $P_G$ ,  $P_{CG}$  and  $P_{Sa}$  (%) are the area coverage of grass land, crop grass land, and savanna land, respectively.  $b_G$ ,  $b_{CG}$  and  $b_{Sa}$  (dimensionless) are the corresponding coefficients (Table S3). The coefficient  $b_G$  represents roughly the fraction of grass land area occupied by ragweed plants, likewise for other coefficients. The details of the calculation of ragweed coverage are provided in Appendix A.

## 2.3. Flowering likelihood

Daily flowering likelihood  $L_d$  was estimated based on the assumption that flowering likelihood increases gradually from the first flowering day to a peak in the middle and then decreases gradually to zero at the end of pollen season. The functional form for the daily flowering likelihood was adapted from the literature (Helbig et al., 2004). It can be parameterized using:

$$L_d(d) = c_b \left( \frac{d}{SL} - \frac{d^2}{SL^2} \right) \quad (8)$$

where  $d$  is number of days from the start date of pollen season,  $SL$  (days) is the season length,  $c_b$  is a normalizing constant which makes  $\sum L_d = 1$ .

The start date and season length of allergenic pollen season in each of modeling grids were simulated based on methods reported in our previous study (Zhang et al., 2015).

A bimodal characteristic has been observed for daily pollen release at flower scale (Martin et al., 2010). This bimodal characteristic reflects mainly the diurnal features of pollen release. For oak, the hourly flowering likelihood  $L_h$  was constructed using two normal distributions with different means and standard deviations as shown in Eq. (9):

$$L_h(t) = \alpha \frac{1}{\sqrt{2\pi}\sigma_d} e^{-\frac{(t-\mu_d)^2}{2\sigma_d^2}} + (1-\alpha) \frac{1}{\sqrt{2\pi}\sigma_n} e^{-\frac{(t-\mu_n)^2}{2\sigma_n^2}}, \quad t = (0, 1, \dots, 23) \quad (9)$$

where  $t$  is hour number,  $\alpha$  and  $1 - \alpha$  are the daytime and nighttime fractions of daily pollen release, respectively,  $\mu_d$  and  $\mu_n$  are the daytime and nighttime means of pollen release time, respectively, and  $\sigma_d$  and  $\sigma_n$  are the daytime and nighttime standard deviations, respectively. These parameters were obtained by fitting the data reported by Pasken and Pietrowicz (2005).

For ragweed, the flowering likelihood  $L_h$  was simulated using the algorithm developed by Martin et al. (2010). This algorithm relates the distributions of pollen emission to the relative humidity and elapsed time after sunrise. For simulation of the hourly flowering likelihood for ragweed in a cell of the model grid, the sunrise time was calculated according to the latitude and longitude of the grid cell; The hourly relative humidity was derived from a climatological simulation of the year 2004 by the Community Earth System Model (CESM), which was down-scaled using the WRF model (Nolte et al., 2018; Spero et al., 2016). The parameters used in Eq. (9) are listed in Table S4.

#### 2.4. Meteorology factors

The meteorological adjustment factor  $K_e$  is primarily related to the friction velocity, which is an important parameter for estimating the turbulent mixing that entrains the pollen from flower to atmosphere. The threshold friction velocity  $u_{*t}$  is required to activate the saltation process leading to dust entrainment. Shao and Lu (2000) introduced a physical parameterization of  $u_{*t}$  for dry and bare soils as shown in Eq. (10):

$$u_{*t} = \left( \alpha_1 \left[ \rho_p g d_p / \rho_a + \alpha_2 / (\rho_a d_p) \right] \right)^{1/2} \quad (10)$$

where factors  $\alpha_1 = 0.0123$  and  $\alpha_2 = 3 \times 10^{-4}$  (kg/s) are defined on the basis of the results obtained from a wind tunnel experiment,  $\rho_p$  (kg/m<sup>3</sup>) and  $\rho_a$  (kg/m<sup>3</sup>) are the pollen and air densities, respectively, and  $d_p$  is the aerodynamic diameter of pollen.

Since pollen is intrinsically different from soil, a modified friction velocity was introduced through Eq. (11) by Helbig et al. (2004) to account for the meteorological effect on pollen emission:

$$\begin{cases} u_{*te} = Au_{*t} \\ u_{*tr} = Bu_{*t} \end{cases} \quad (11)$$

where  $A$  and  $B$  are the meteorological coefficients for direct emission and resuspension emission, respectively. They were further parameterized using Eq. (12):

$$\begin{cases} A = \frac{3}{\alpha_T + \alpha_U + \alpha_V} \\ B = \frac{2}{\beta_U + \beta_V} \end{cases} \quad (12)$$

where  $\alpha_T$ ,  $\alpha_U$  and  $\alpha_V$  are the resistances due to temperature  $T$  (°C), relative humidity  $U$  (%) and wind speed  $V$  (m/h) at 10 m, respectively;  $\beta_U$  and  $\beta_V$  are the corresponding resistances for resuspension emission.

The three resistances were further parameterized using Eq. (13):

$$\begin{cases} \alpha_T = c_{Te} T / T_{te}, & \alpha_U = c_{Ue} U_{te} / U, & \alpha_V = c_{Ve} V / V_{te} \\ \beta_U = c_{Ur} U_{tr} / U, & \beta_V = c_{Vr} V / V_{tr} \end{cases} \quad (13)$$

where  $c_{Te}$ ,  $c_{Ue}$  and  $c_{Ve}$  are species specific constants, and  $T_{te}$ ,  $U_{te}$  and  $V_{te}$  are the threshold values of temperature, relative humidity and wind speed for direct pollen emission.  $c_{Ur}$ ,  $c_{Vr}$ ,  $U_{tr}$  and  $V_{tr}$  are the corresponding constants and threshold values for resuspension emission.

Finally, the meteorological adjustment factors  $K_e$  and  $K_r$  were calculated through Eq. (14) (Helbig et al., 2004):

$$\begin{cases} K_e = 1 - e^{-u_{*t}/u_{*te}} \\ K_r = 1 - e^{-u_{*t}/u_{*tr}} \end{cases} \quad (14)$$

which indicates that higher ground surface temperature, wind speed, and lower humidity favor pollen release. We did not assume a cutoff threshold velocity determining whether pollen particles can be released or not. Instead, Eq. (14) indicates that the higher the friction velocity is, a higher proportion of pollen is released.

#### 2.5. Deposition velocity

Deposition velocity was calculated using a resistance model as presented in Eq. (15) (Seinfeld and Pandis, 1997):

$$v_d = \frac{1}{r_a + r_b + r_a r_b v_s} + v_s \quad (15)$$

where  $r_a$  and  $r_b$  (h/m) are the aerodynamic resistance and quasi-laminar resistance, respectively.  $v_s$  (m/h) is the settling velocity, which was calculated using Stokes' Equation:

$$v_s = \frac{\rho_p d_p^2 g C_c}{18\mu} \quad (16)$$

where air dynamic viscosity  $\mu$  is approximately  $1.8 \times 10^{-5}$  kg/(m s) (Sofiev et al., 2006).  $C_c$  is the slip correction factor used to correct the non-continuum effects of particles in the air according to their diameters (Seinfeld and Pandis, 1997). In the current study, it takes the value of 1.008 for pollen grains, which have an average aerodynamic diameter of around 20  $\mu$ m.

The aerodynamic resistance  $r_a$  and quasi-laminar resistance  $r_b$  were calculated using Eq. (17) (Seinfeld and Pandis, 1997):

$$\begin{cases} r_a = \frac{\ln(H_C/Z_0)}{\kappa u_*} \\ r_b = \frac{1}{u_* (Sc^{-2/3} + 10^{-3/St})} \end{cases} \quad (17)$$

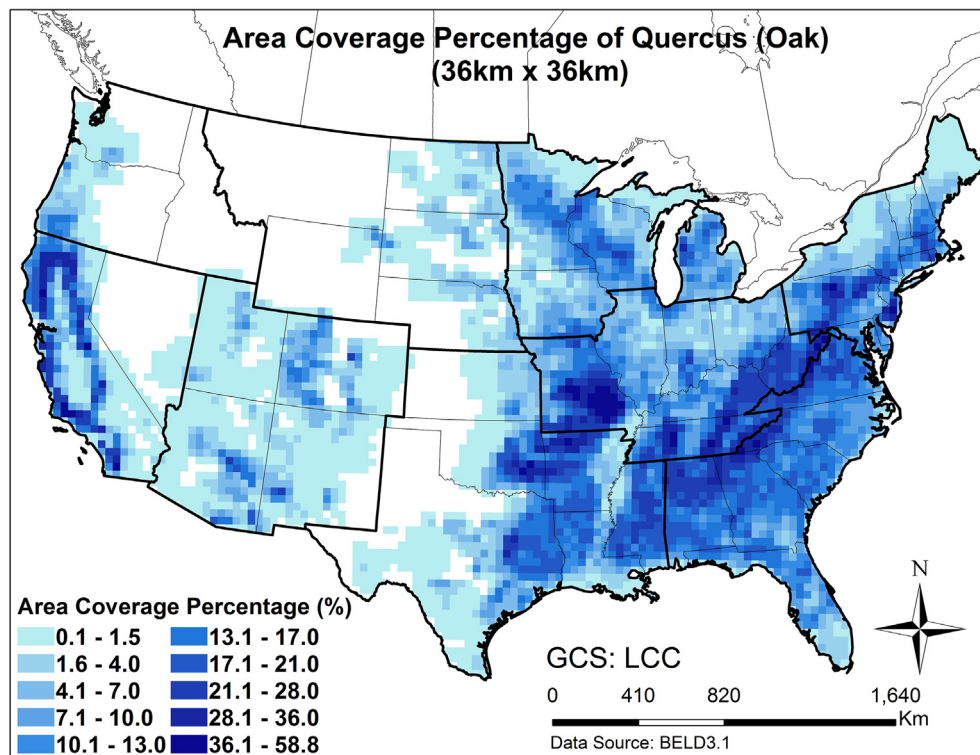
where  $\kappa = 0.41$  is the von Karman constant;  $Sc = \gamma/D$  is the Schmidt number;  $St = v_s u_*^2 / (g\gamma)$  is the Stokes number;  $D = k_B T C_c / (3\pi\mu d_p)$  is the molecular diffusivity, and  $\gamma = \mu/\rho_a$  is the kinematic viscosity.

#### 2.6. Spatiotemporal pattern of allergenic pollen emission

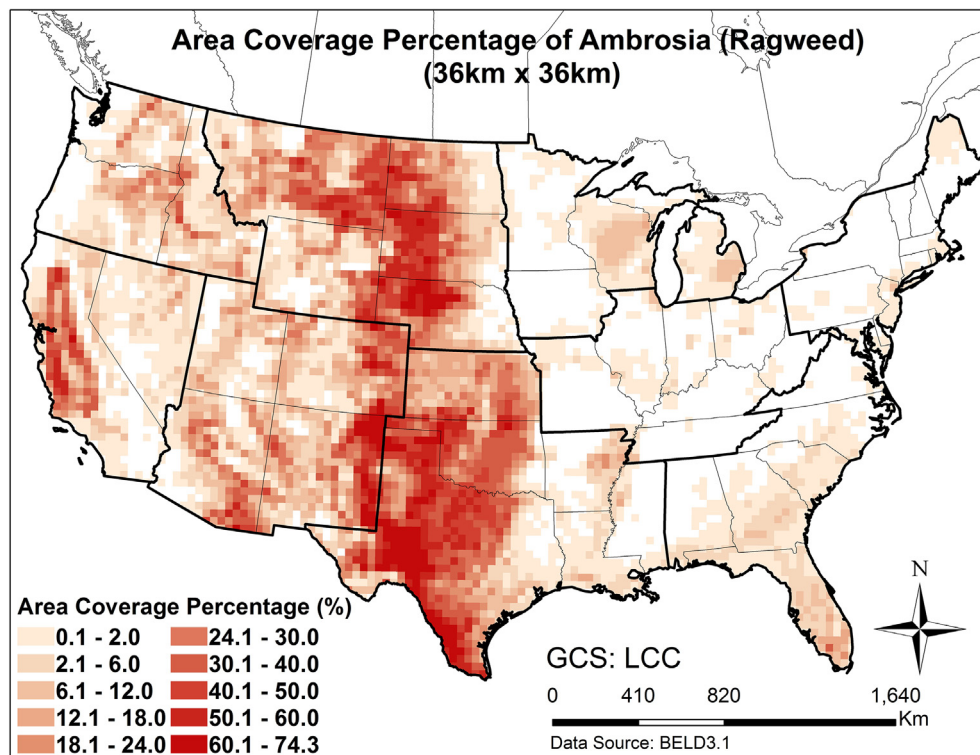
For oak, the emission model was run from 1 March to 30 April 2004 with 36-km horizontal grid spacing over the CONUS and temporal resolution of 1 h. For ragweed, the emission model was run from 1 August to 30 September 2004 covering the same domain with the same resolution.

For investigation of the spatiotemporal pattern, the mean ( $F_{g,hrMn}$ ), maximum ( $F_{g,hrMx}$ ), seasonal total ( $F_{g,hrSum}$ ) and standard deviation ( $F_{g,hrStd}$ ) of the simulated hourly emission in each cell of the modeling





(a)



(b)

**Fig. 2.** Area coverage of: (a) oak and (b) ragweed with 36-km horizontal grid spacing over the CONUS. Area coverage for oak was generated using Spatial Allocator (Eyth and Habisak, 2003) to redistribute the BELD3.1 data with 1-km grid resolution into 36-km grid resolution. Area coverage for ragweed was generated using the algorithm developed in the current study.

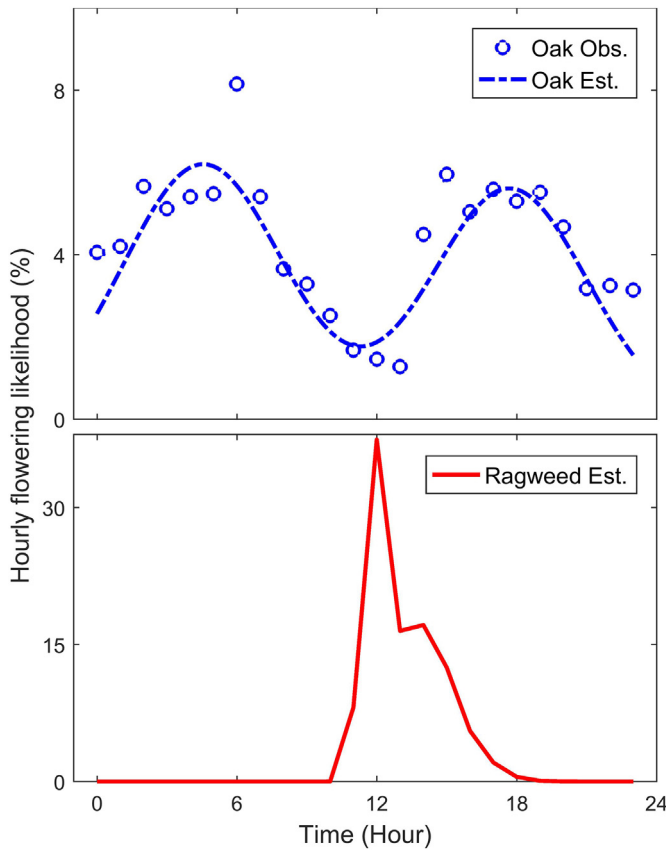


Fig. 3. Simulated hourly flowering likelihood for oak (top) and ragweed (bottom).

grid were calculated using Eq. (18):

$$\begin{cases} F_{g,hrMn}(i,j) = \frac{\sum_t F_g(i,j,t)}{N_t} \\ F_{g,hrMx}(i,j) = \max_t F_g(i,j,t) \\ F_{g,hrSum}(i,j) = \sum_t F_g(i,j,t) \\ F_{g,hrStd}(i,j) = \sqrt{\frac{\sum_t (F_g(i,j,t) - F_{g,hrMn}(i,j))^2}{N_t}} \end{cases} \quad (18)$$

where  $F_g(i,j,t)$  is the pollen emission flux in grid cell  $(i,j)$  at time  $t$ ;  $N_t$  is a temporal index for time  $t$ . These four emission metrics  $F_{g,hrMn}$ ,  $F_{g,hrMx}$ ,  $F_{g,hrSum}$  and  $F_{g,hrStd}$ , hereafter are also sometimes referred to as hourly mean, hourly maximum, seasonal total and standard deviation of pollen emission, respectively.

### 2.7. Sensitivity analysis

Global sensitivity analyses were performed to test the sensitivity of the pollen emission model to multiple inputs and parameters based on Morris's design (Morris, 1991). This design estimates the main effect of a parameter by computing a number of local sensitivities at random points of the parameter space. The mean of these randomized local sensitivities indicates the overall influence of a given parameter on the output metric, while the corresponding standard deviation indicates the effects of interaction and nonlinearity (Saltelli et al., 2000).

The regional mean hourly emission ( $F_{hrMn}$ ) was selected as a metric for testing the emission model's sensitivity to multiple inputs and parameters. The definition of this metric is presented in Eq. (19):

$$F_{hrMn} = \frac{\sum_{i,j,t} F_g(i,j,t)}{N_i N_j N_t} \quad (19)$$

where  $N_i$  and  $N_j$  are the values of spatial indices  $i$  and  $j$ , respectively.

In the current study, each of the 23 parameters (Table 1) was sampled 6000 times according to Morris' method from 250 random trajectories (each has 24 steps) in the parameter space (Morris, 1991; Saltelli et al., 2000). Each of the parameters was perturbed between 50% and 150% of its base value or distribution while keeping other parameters unchanged. Eq. (20) was used to calculate the Normalized Sensitivity Coefficient (NSC) for regional hourly mean emission at a local point:

$$NSC_{hrMn} = \frac{\Delta F_{hrMn} / F_{hrMn}}{\Delta P / P} \quad (20)$$

where  $F_{hrMn}$  and  $P$  are the regional mean hourly emission flux and the input parameter, respectively; and  $\Delta F_{hrMn}$  and  $\Delta P$  are the perturbations in the emission flux and input parameters, respectively.

The global NSC of a parameter, NSCg, is defined as the mean of the corresponding local sensitivity. The average absolute global NSC,  $|\overline{NSCg}|$ , for each parameter and pollen taxon can be derived based on the means of the absolute NSCg. Similarly, the standard deviations averaged over each parameter and pollen taxon ( $STD$ ) can be obtained to evaluate the interactions and nonlinearity effects of input parameters on modeling output.

### 2.8. Qualitative evaluation of the emission model

Since the emission fluxes are not monitored or measured in the field for the CONUS, the qualitative evaluation of model performance was conducted based on known distributions of plants and observed pollen counts. Correlation analysis of the simulated seasonal total pollen emissions at each cell of the modeling grid and the corresponding plant coverages was done after the data were normalized with mean zero and unit standard deviation. The correlation of normalized annual total pollen counts at pollen monitoring stations with the corresponding normalized simulated seasonal total emission was evaluated similarly.

## 3. Results and discussion

### 3.1. Vegetation coverage

Fig. 2 presents the percentage of the area occupied by oak and ragweed in each cell of the modeling grid covering the CONUS. Oak trees are distributed mostly across eight of the nine climate regions of the CONUS with the highest area coverages (36%–58.8%) in the West, Central and Southeast climate regions. Ragweed is mainly distributed in the western US, with the highest area coverages (60.1%–74.3%) in the South and the West North Central climate regions. The classification of the nine climate regions across the CONUS is illustrated in Fig. S3. These vegetation coverage maps are important inputs to the pollen emission model, which were used in Eq. (6) to calculate the pollen emission fluxes in each cell of the modeling grid covering the CONUS.

### 3.2. Flowering likelihood

Fig. 3 shows patterns of the simulated hourly flowering likelihood for oak and ragweed. Table S4 lists the parameters and references for calculating the hourly flowering likelihood. The hourly flowering likelihood of oak was derived from observed hourly pollen counts reported in the literature; these were derived using maximum likelihood estimation (Pasken and Pietrowicz, 2005). The bimodal features of hourly flowering likelihood observed in Fig. 3 for oak reflect the pollen emissions in early morning and late afternoon. The simulated hourly flowering likelihood captures the main features observed in the hourly pollen counts. For ragweed, the hourly flowering likelihood was modeled based on the physiological characteristics of ragweed via direct observation of the floral development and morphology. This model also relates the distributions of pollen emission to the relative humidity and

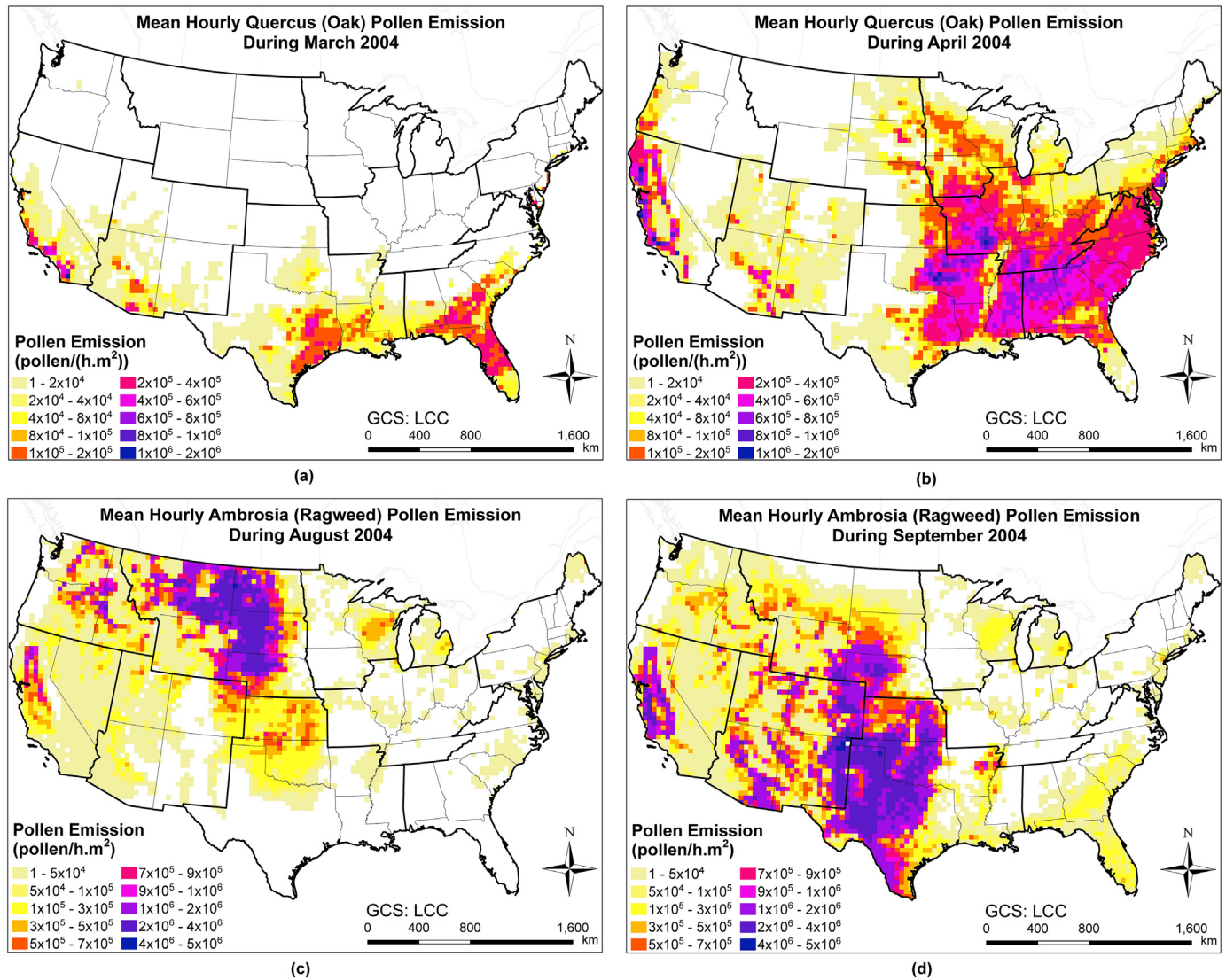


**Fig. 4.** Spatial patterns of mean hourly emission of (a) oak pollen in March 2004; (b) oak pollen in April 2004; (c) ragweed pollen in August 2004; and (d) ragweed pollen in September 2004.

elapsed time after sunrise (Martin et al., 2010). A recent study by Šikoparija et al. (2018) observed similar diurnal pattern of ragweed pollen emission by direct continuous measurements of the ragweed pollen concentration in the field during the flowering season. This field experiment collected ragweed pollen samples near the canopy level of the ragweed field with high temporal resolution. Thus, it was able to capture the diurnal variation of pollen emission. They also found that the shape of the diurnal cycle is affected by meteorological conditions such as relative humidity.

### 3.3. Spatiotemporal pattern of allergenic pollen emission

To examine the temporal pattern of pollen emission, the mean hourly emission fluxes over the early and late flowering period for oak and ragweed are plotted in Fig. 4. Oak pollen emissions started from the Southern CONUS in March and then shifted gradually toward the Northern CONUS in April. In contrast to oak, ragweed pollen emissions started from the Northern CONUS in August and then shifted gradually toward the Southern CONUS in September. This pattern is consistent with long term observations (Zhang et al., 2015; Ziska et al., 2011), and is simulated for the first time in this study. It has been identified that summer-flowering ragweed has earlier flower initiation at high latitudes than lower latitudes, which is a typical adaption to the

environment to maximize reproductive success (Stinson et al., 2016). The time slices of pollen emissions in Fig. 5 display the diurnal variation of pollen emission. In general, the oak pollen emission flux in each cell of the modeling grid at 11:00 UTC is higher than that at 18:00 UTC (averaged over Apr 21–Apr 30, 2004), and the ragweed pollen emission flux in each cell of the modeling grid at 14:00 UTC is higher than that at 18:00 UTC (averaged over Sept 21–Sept 30, 2004), which is mainly caused by variation of hourly flowering likelihood. The emission model developed in this study demonstrated the daily and hourly variation of pollen emission flux due to the intrinsic physiological characteristics of the plants and influences of meteorological factors such as temperature, wind velocity and relative humidity.

Fig. 6 depicts the spatial patterns of oak pollen emissions during the entire pollen season in 2004. The spatial patterns were examined for four metrics: mean, maximum, seasonal total, and standard deviation of hourly emissions at each cell of the modeling grid covering the CONUS. These four metrics were calculated using Eq. (18) based on the simulated hourly emissions of oak pollen between 1 March 2004 and 30 April 2004. The spatial patterns of mean, maximum, seasonal and standard deviation of hourly emission flux all roughly follow the pattern of area coverage of oak trees shown in Fig. 2. The oak pollen emissions varied substantially in different climate regions. The seasonal total oak pollen emissions in the Southeast, South and Central climate



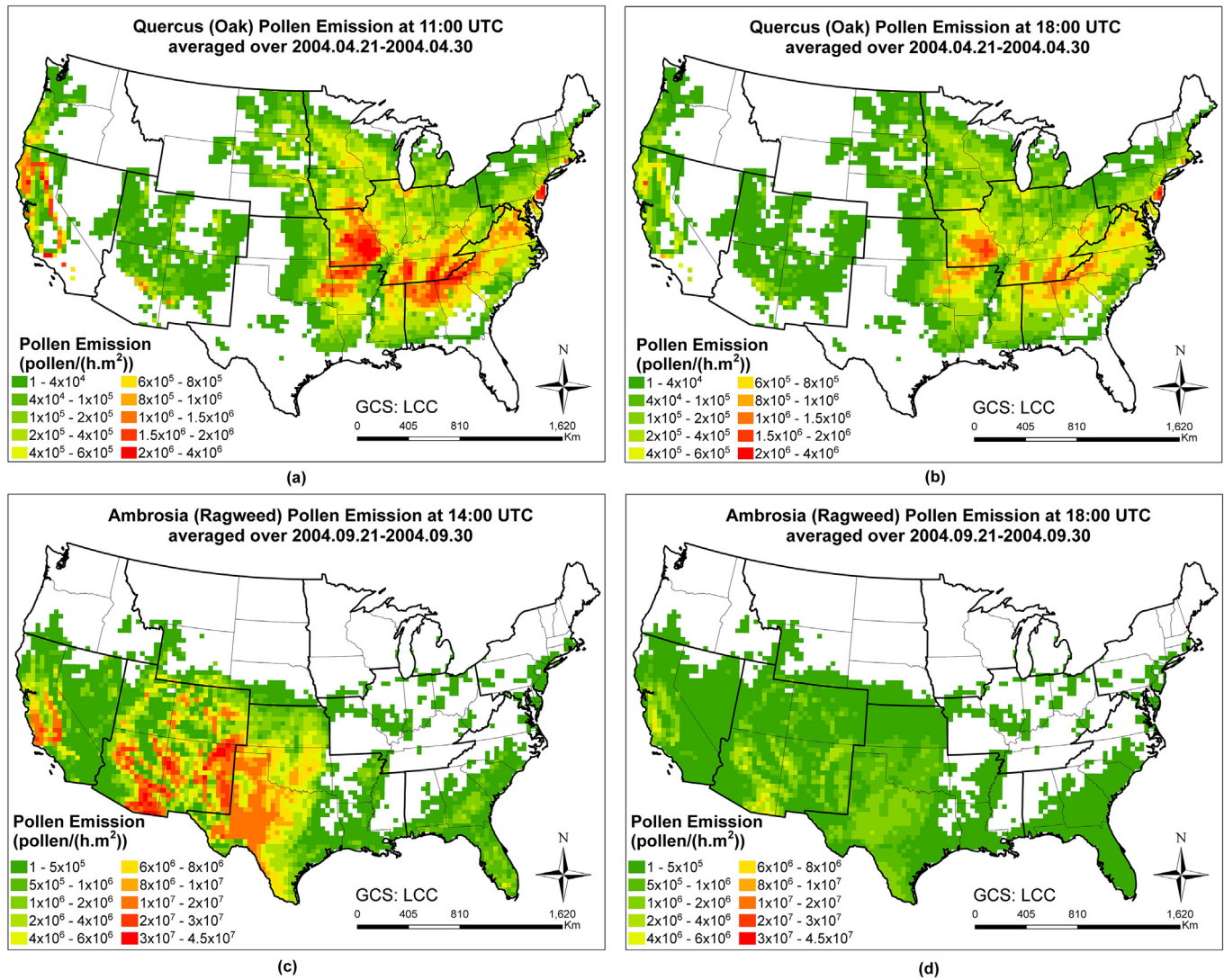


**Fig. 5.** Time slices of spatiotemporal emission profiles of (a) oak pollen at 11:00 UTC (averaged over Apr 21–Apr 30, 2004); (b) oak pollen at 18:00 UTC (averaged over Apr 21–Apr 30, 2004); (c) ragweed pollen at 14:00 UTC (averaged over Sept 21–Sept 30, 2004); and (d) ragweed pollen at 18:00 UTC (averaged over Sept 21–Sept 30, 2004).

regions were higher than those in other regions in the CONUS. The mean hourly oak emission flux can increase up to  $9 \times 10^5$  pollen/( $\text{m}^2 \text{ h}$ ). The maximum hourly oak pollen emission flux was  $5.8 \times 10^6$  pollen/( $\text{m}^2 \text{ h}$ ). As shown in Fig. S4, the spatial patterns of ragweed emission flux also follow the patterns of ragweed area coverage. The South and West North Central climate regions had the highest ragweed seasonal total emission of  $4 \times 10^9$  pollen/ $\text{m}^2$ . The standard deviations of the hourly pollen emission flux throughout the season were caused by variations in daily and hourly flowering likelihood, and the meteorological factors contributing to pollen emission. The mean hourly ragweed pollen emission can reach up to  $2.4 \times 10^6$  pollen/( $\text{m}^2 \text{ h}$ ). The magnitude of the simulated pollen emission flux is comparable to that reported by Šikoparija et al. (2018), which were obtained through an empirical study. The observed average hourly ragweed pollen emission flux was derived from direct measurements of airborne pollen concentrations in the field and ranged from  $2.7 \times 10^6$  pollen/( $\text{m}^2 \text{ h}$ ) to  $3.2 \times 10^8$  pollen/( $\text{m}^2 \text{ h}$ ).

### 3.4. Sensitivity analysis

The global sensitivity of the simulated regional mean hourly pollen emissions to different parameters is presented in Fig. 7. The global NSC of all parameters, except the density of oak pollen grain

( $\rho_p$ ), varied within  $-0.1$  and  $0.1$  for pollen emissions from oak. The average absolute global NSC of density of oak pollen grain ( $\rho_p$ ) is  $0.1311$ . The ragweed pollen emission model is also robust to 22 of the 23 parameters ( $-0.1 < \text{global NSC} < 0.1$ ), but more sensitive to diameter of pollen grain ( $d_p$ ), with an average absolute global NSC of  $0.1438$ .

The standard deviations of NSCs for pollen emissions of oak and ragweed were between  $0.4626$  and  $0.6836$ . This indicated low interaction and nonlinearity effects among parameters for pollen emissions of oak and ragweed.

Uncertainties in sensitive and interactive input parameters can result to large deviations of model predictions. In particular, we acknowledge that there are substantial uncertainties in dry deposition velocity (Eq. (15)), plant area coverage (Eq. (7)), flowering likelihood (Eq. (9)), and our assumptions of quasi-steady state and quasi-equilibrium balance of pollen fluxes (Eq. (2)). A new parameterization of deposition velocity has been developed similar to that in Zhang and Shao (2014) and Zhang and He (2014). Particularly, deposition velocity for large particles such as pollen still has substantial uncertainties, and will need to be further investigated. Plant area coverages calculated using land use data in combination with annual pollen counts seem more reasonable than those calculated based on plant inventory or ecological model (Zink et al., 2016).



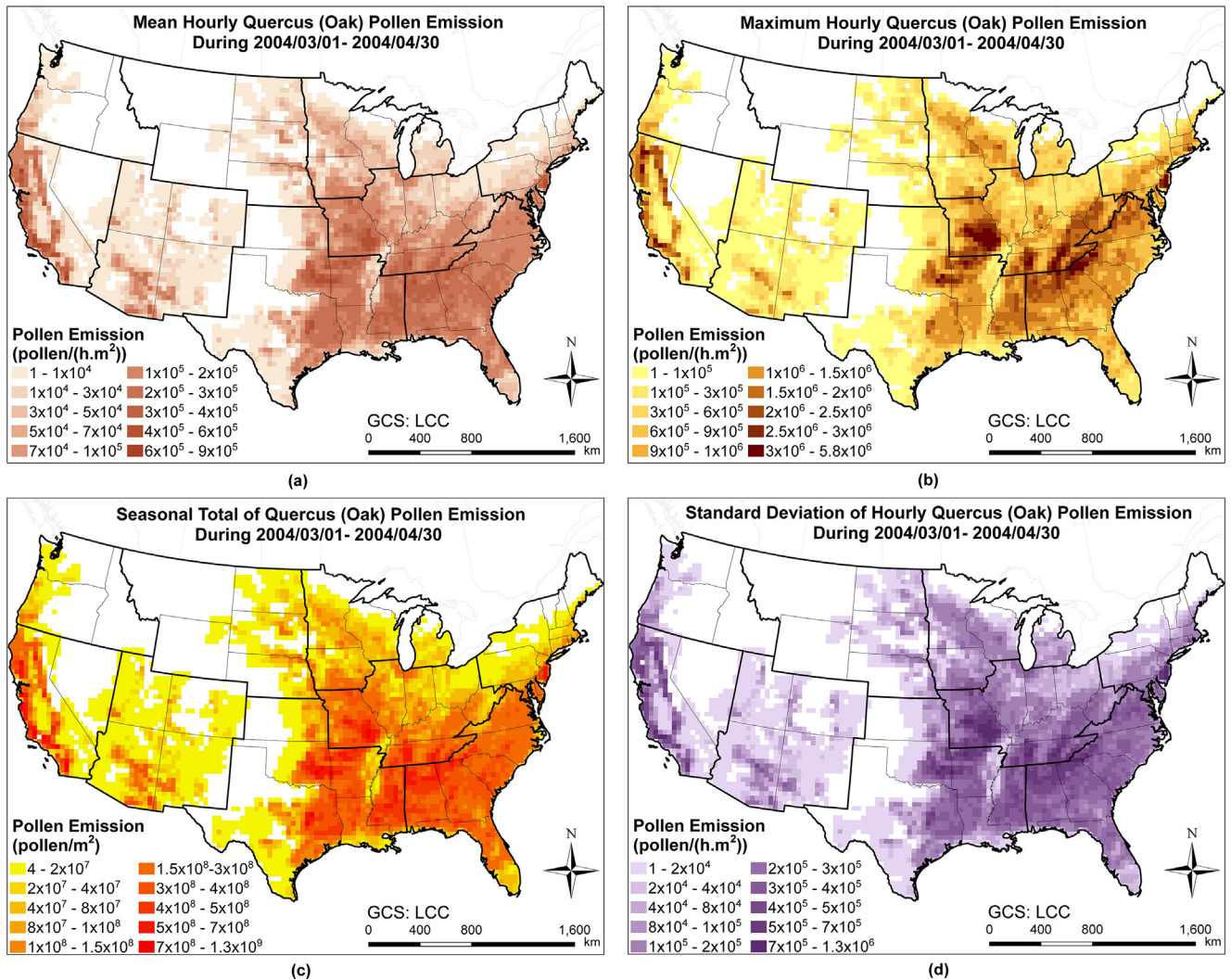


**Fig. 6.** Spatial patterns of mean, maximum, seasonal total and standard deviation of hourly emission of oak pollen. (a) Hourly mean, (b) hourly maximum, (c) seasonal total, and (d) standard deviation.

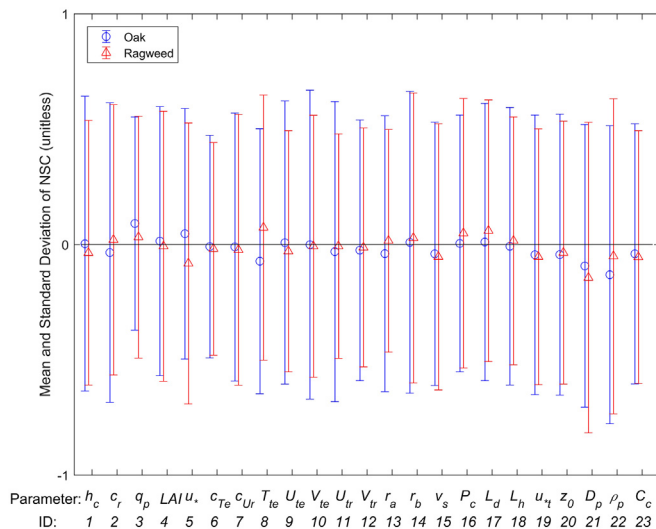


**Fig. 7.** Mean and standard deviation of Normalized Sensitivity Coefficient (NSC) for each parameter for the pollen emission model of oak and ragweed. All parameters are described in Table 1.

### 3.5. Evaluation of model performance

To investigate the accuracy of the simulated pollen emissions with respect to plant coverage, scatterplots of normalized coverage and seasonal total emission for oak and ragweed pollen are shown in Fig. 8. The Pearson correlation coefficients for oak is 0.813 ( $p$ -value  $< 0.0001$ ), and 0.892 ( $p$ -value  $< 0.0001$ ) for ragweed. The data points should fall on or near the 45-degree line in Fig. 8 if there is linear relationship between the two normalized variables. The deviations from the diagonal line are caused by various factors such as temperature, humidity, wind speed, etc. that were fully considered in the emission model. The correlation of observed annual total pollen counts at selected pollen monitoring stations with the corresponding simulated seasonal total emission is illustrated in Fig. 9. Due to the incompleteness of pollen observations at the monitoring stations in 2004, only stations with  $>20$  days of valid observations were selected. Data from 36 monitoring stations for oak show a Pearson correlation coefficient of 0.421 ( $p$ -value is 0.0105), while data from 34 monitoring stations for ragweed result in a Pearson correlation coefficient of 0.787 ( $p$ -value  $< 0.0001$ ). Pollen counts at monitoring stations are affected not only by pollen emission, but also by atmospheric transport of pollen, which will be incorporated and simulated in a new pollen transport model that is currently being developed and tested by our group.

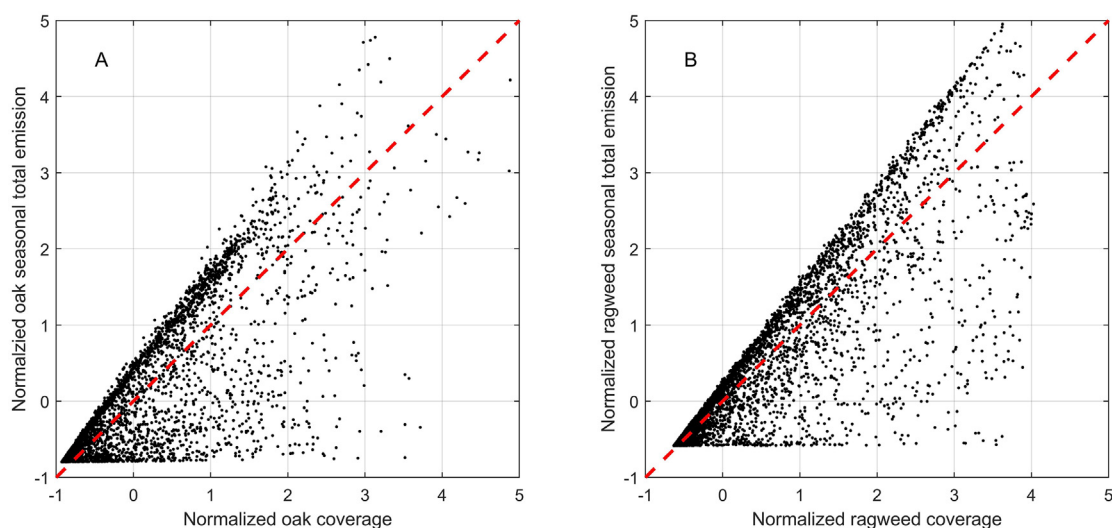


Fig. 8. Scatterplot of normalized coverage and normalized seasonal total emission in 2004 for oak and ragweed pollen with 45-degree line.

#### 4. Conclusion

The present study described the development of a new semi-mechanistic emission model for allergenic pollen and tested the model performance for oak and ragweed. This model was derived through application of mass balance of pollen grain fluxes in the immediate surroundings of allergenic plants. It considers the physiological characteristics of the plants, consists of direct emission and resuspension, and accounts for influences of temperature, wind velocity and relative humidity. Modules of this emission model have been developed and parameterized using data driven statistical modeling with multiple years of observed daily pollen counts to provide pollen season onset and duration, hourly flowering likelihood, and vegetation coverage. The simulated spatiotemporal patterns of pollen emissions generally follow the corresponding patterns of area coverage of allergenic plants and diurnal patterns of hourly flowering likelihood. This study, for the first time, simulated the ragweed pollen onset pattern that starts from the cold north and transits to the warm south. A systematic sensitivity analysis showed that the emission model presented here is robust with respect to parameterizations developed for the emission of oak and ragweed pollen. Qualitative evaluations of the model performance

revealed that the simulated emission of oak and ragweed pollen are strongly correlated with their spatial distributions over CONUS and the observed pollen counts at pollen monitoring stations. Pollen emissions are crucial inputs for pollen transport modeling, which could also quantitatively evaluate the emission model. The transport of pollen will be simulated using an adapted CMAQ model, which is the subject of our next paper.

#### Acknowledgements

This research was funded in part by the U.S. Environmental Protection Agency (EPA) under STAR Grant EPA-RD-83454701-0 to Rutgers University, by the NIEHS sponsored Center for Environmental Exposures and Disease at EOHSI (P30ES005022), and by the Ozone Research Center which is funded by the State of New Jersey Department of Environmental Protection. Drs. Gao and Leung are supported by the U.S. Department of Energy Office of Science Regional and Global Climate Modeling program. Pacific Northwest National Laboratory is operated for DOE by Battelle Memorial Institute under contract DE-AC05-76RL01830. We thank NAB for providing airborne pollen data, and Ms. Linda Everett and Mr. George M. Grindlinger (Rutgers) for editorial

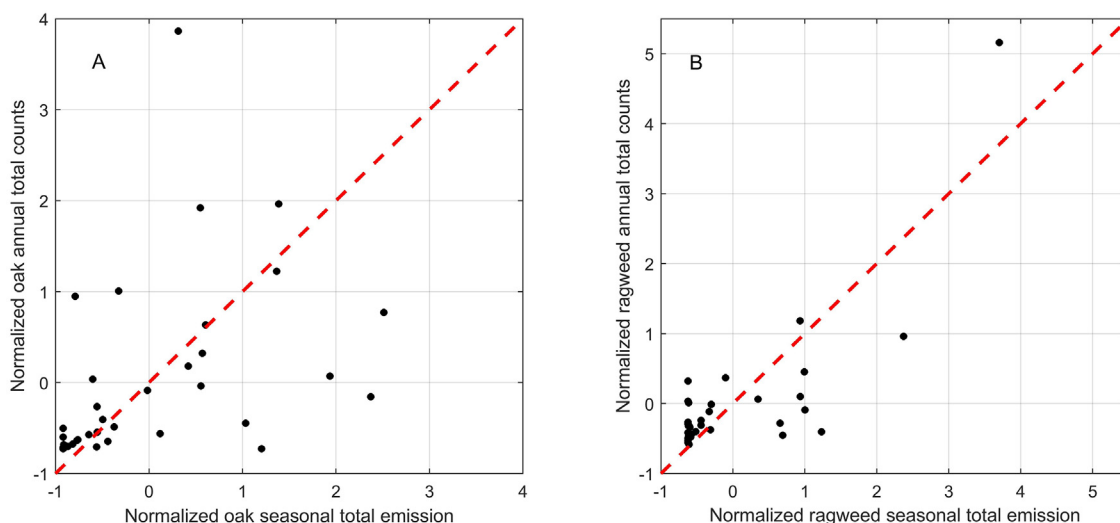


Fig. 9. Scatterplot of normalized annual pollen counts observation and normalized seasonal total emission in 2004 for oak and ragweed pollen with 45-degree line.

and technical assistance. The views expressed in this article are those of the authors and do not necessarily represent the views or policies of the U.S. EPA.

## Appendix A. Supplementary data

Supplementary data to this article can be found online at <https://doi.org/10.1016/j.scitotenv.2018.10.243>.

## References

- Adhikari, A., Reponen, T., Grinshpun, S.A., Martuzevicius, D., LeMasters, G., 2006. Correlation of ambient inhalable bioaerosols with particulate matter and ozone: a two-year study. *Environ. Pollut.* 140, 16–28.
- Bielory, L., Lyons, K., Goldberg, R., 2012. Climate change and allergic disease. *Curr Allergy Asthma Rep* 12, 485–494.
- Breton, M.-C., Garneau, M., Fortier, I., Guay, F., Louis, J., 2006. Relationship between climate, pollen concentrations of Ambrosia and medical consultations for allergic rhinitis in Montreal, 1994–2002. *Sci. Total Environ.* 370, 39–50.
- Brose, P., Van Lear, D., Cooper, R., 1999. Using shelterwood harvests and prescribed fire to regenerate oak stands on productive upland sites. *For. Ecol. Manag.* 113, 125–141.
- Cakmak, S., Dales, R.E., Burnett, R.T., Judek, S., Coates, F., Brook, J.R., 2002. Effect of airborne allergens on emergency visits by children for conjunctivitis and rhinitis. *Lancet* 359, 947–948.
- Cakmak, S., Dales, R.E., Coates, F., 2012. Does air pollution increase the effect of aeroallergens on hospitalization for asthma? *J. Allergy Clin. Immunol.* 129, 228–231.
- Chamecki, M., Meneveau, C., Parlange, M.B., 2009. Large eddy simulation of pollen transport in the atmospheric boundary layer. *J. Aerosol Sci.* 40, 241–255.
- Cornai, G., Mikus, G., Nádor, G., Hubik, I., László, I., Suba, Z., 2010. In: Gartner, G., Ortig, F. (Eds.), *Integration of Hightech Components for Operating Ragweed Mapping and Control System in Hungary Using Remote Sensing and GIS Cartography in Central and Eastern Europe*. Springer Berlin Heidelberg, pp. 405–415.
- Dales, R.E., Cakmak, S., Judek, S., Dann, T., Coates, F., Brook, J.R., et al., 2004. Influence of outdoor aeroallergens on hospitalization for asthma in Canada. *J. Allergy Clin. Immunol.* 113, 303–306.
- Davis, M.B., Brubaker, L.B., 1973. Differential sedimentation of pollen grains in lakes. *Limnol. Oceanogr.* 18, 635–646.
- Deen, W., Swanton, C.J., Hunt, L.A., 2001. A mechanistic growth and development model of common ragweed. *Weed Sci.* 49, 723–731.
- Efstathiou, C., Isukapalli, S., Georgopoulos, P., 2011. A mechanistic modeling system for estimating large scale emissions and transport of pollen and co-allergens. *Atmos. Environ. (Oxford, England: 1994)* 45, 2260–2276.
- Eyth, A.M., Habisak, K., 2003. The MIMS spatial allocator: a tool for generating emission surrogates without a geographic information system. *Proceedings, 12th International Emission Inventory Conference, San Diego*.
- Foster, M.M., Vitousek, P.M., Randolph, P.A., 1980. Effects of ragweed (*Ambrosia-Artemisiifolia* L.) on nutrient cycling in a 1st-year old-field. *Am. Midl. Nat.* 103, 106–113.
- Fumanal, B., Chauvel, B., Bretagnolle, F., 2007. Estimation of pollen and seed production of common ragweed in France. *Ann. Agric. Environ. Med.* 14, 233–236.
- Helbig, N., Vogel, B., Vogel, H., Fiedler, F., 2004. Numerical modelling of pollen dispersion on the regional scale. *Aerobiologia* 20, 3–19.
- Kawashima, S., Takahashi, Y., 1999. An improved simulation of mesoscale dispersion of airborne cedar pollen using a flowering-time map. *Grana* 38, 316–324.
- Kim, K.H., Jahan, S.A., Kabir, E., 2013. A review on human health perspective of air pollution with respect to allergies and asthma. *Environ. Int.* 59, 41–52.
- Kinnee, E., Geron, C., Pierce, T., 1997. United States land use inventory for estimating biogenic ozone precursor emissions. *Ecol. Appl.* 7, 46–58.
- Martin, M.D., Chamecki, M., Brush, G.S., 2010. Anthesis synchronization and floral morphology determine diurnal patterns of ragweed pollen dispersal. *Agric. For. Meteorol.* 150, 1307–1317.
- Morris, M.D., 1991. Factorial sampling plans for preliminary computational experiments. *Technometrics* 33, 161–174.
- Nolte, C.G., Spero, T.L., Bowden, J.H., Mallard, M.S., Dolwick, P.D., 2018. The potential effects of climate change on air quality across the conterminous US at 2030 under three Representative Concentration Pathways. *Atmos. Chem. Phys.* 18, 15471–15489. <https://doi.org/10.5194/acp-18-15471-2018>.
- Pasken, R., Pietrowicz, J.A., 2005. Using dispersion and mesoscale meteorological models to forecast pollen concentrations. *Atmos. Environ.* 39, 7689–7701.
- Pauling, A., Rotach, M., Gehrig, R., Clot, B., Network, CttEA, 2012. A method to derive vegetation distribution maps for pollen dispersion models using birch as an example. *Int. J. Biometeorol.* 56, 949–958.
- Prank, M., Chapman, D.S., Bullock, J.M., Belmonte, J., Berger, U., Dahl, A., et al., 2013. An operational model for forecasting ragweed pollen release and dispersion in Europe. *Agric. For. Meteorol.* 182–183, 43–53.
- Saltelli, A., Chan, K., Scott, E.M., 2000. *Sensitivity Analysis*. vol. 134. Wiley, New York.
- Schueler, S., Schlünzen, K., 2006. Modeling of oak pollen dispersal on the landscape level with a mesoscale atmospheric model. *Environ. Model. Assess.* 11, 179–194.
- Seinfeld, J.H., Pandis, S.N., 1997. *Atmospheric Chemistry and Physics: From Air Pollution to Climate Change*. John Wiley & Sons.
- Shao, Y., Lu, H., 2000. A simple expression for wind erosion threshold friction velocity. *J. Geophys. Res.* 105, 22437–22443.
- Šikoparija, B., Mimić, G., Panić, M., Marko, O., Radišić, P., Pejak-Šikoparija, T., et al., 2018. High temporal resolution of airborne Ambrosia pollen measurements above the source reveals emission characteristics. *Atmos. Environ.* 192, 13–23.
- Siljamo, P., Sofiev, M., Filatova, E., Grewling, L., Jäger, S., Khoreva, E., et al., 2013. A numerical model of birch pollen emission and dispersion in the atmosphere. Model evaluation and sensitivity analysis. *Int. J. Biometeorol.* 57, 125–136.
- Skjøth, C.A., Smith, M., Šikoparija, B., Stach, A., Myszkowska, D., Kasprzyk, I., et al., 2010. A method for producing airborne pollen source inventories: an example of Ambrosia (ragweed) on the Pannonian Plain. *Agric. For. Meteorol.* 150, 1203–1210.
- Sofiev, M., Bergmann, K.-C., 2013. *Allergenic Pollen: A Review of the Production, Release, Distribution and Health Impacts*. Springer 9400748817.
- Sofiev, M., Siljamo, P., Ranta, H., Rantio-Lehtimäki, A., 2006. Towards numerical forecasting of long-range air transport of birch pollen: theoretical considerations and a feasibility study. *Int. J. Biometeorol.* 50, 392–402.
- Sofiev, M., Siljamo, P., Ranta, H., Linkosalo, T., Jaeger, S., Rasmussen, A., et al., 2013. A numerical model of birch pollen emission and dispersion in the atmosphere. Description of the emission module. *Int. J. Biometeorol.* 57, 45–58.
- Sofiev, M., Berger, U., Prank, M., Vira, J., Arteta, J., Belmonte, J., et al., 2015. MACC regional multi-model ensemble simulations of birch pollen dispersion in Europe. *Atmos. Chem. Phys. Discuss.* 15, 8243–8281.
- Spero, T.L., Nolte, C.G., Bowden, J.H., Mallard, M.S., Herwehe, J.A., 2016. The impact of incongruous lake temperatures on regional climate extremes downscaled from the CMIP5 archive using the WRF model. *J. Clim.* 29, 839–853.
- Stinson, K.A., Albertine, J.M., Hancock, L.M.S., Seidler, T.G., Rogers, C.A., 2016. Northern ragweed ecotypes flower earlier and longer in response to elevated CO<sub>2</sub>: what are you sneezing at? *Oecologia* 182, 587–594.
- Vogel, H., Pauling, A., Vogel, B., 2008. Numerical simulation of birch pollen dispersion with an operational weather forecast system. *Int. J. Biometeorol.* 52, 805–814.
- Wang, Y.S., Miller, D.R., Welles, J.M., Heisler, G.M., 1992. Spatial variability of canopy foliage in an oak forest estimated with fisheye sensors. *For. Sci.* 38, 854–865.
- Zhang, L., He, Z., 2014. Technical note: an empirical algorithm estimating dry deposition velocity of fine, coarse and giant particles. *Atmos. Chem. Phys.* 14, 3729–3737.
- Zhang, J., Shao, Y., 2014. A new parameterization of particle dry deposition over rough surfaces. *Atmos. Chem. Phys.* 14, 12429–12440.
- Zhang, Y., Bielory, L., Cai, T., Mi, Z., Georgopoulos, P., 2015. Predicting onset and duration of airborne allergenic pollen season in the United States. *Atmos. Environ.* 103, 297–306.
- Zink, K., Vogel, H., Vogel, B., Magyar, D., Kottmeier, C., 2012. Modeling the dispersion of *Ambrosia artemisiifolia* L. pollen with the model system COSMO-ART. *Int. J. Biometeorol.* 56, 669–680.
- Zink, K., Kaufmann, P., Petitpierre, B., Broennimann, O., Guisan, A., Gentilini, E., et al., 2016. Numerical ragweed pollen forecasts using different source maps: a comparison for France. *Int. J. Biometeorol.* 1–11.
- Ziska, L., Knowlton, K., Rogers, C., Dalan, D., Tierney, N., Elder, M.A., et al., 2011. Recent warming by latitude associated with increased length of ragweed pollen season in central North America. *Proc. Natl. Acad. Sci. U. S. A.* 108, 4248–4251.